Summer 6-9-2022

Augmented formic acid electro-oxidation at a co-electrodeposited Pd/Au nanoparticle catalyst

Yaser M. Asal
The British University in Egypt

Ahmad M. Mohammad
Cairo University

Sayed S. Abd El Rehim
Ain Shams University

Islam M. Al-Akraa
The British University in Egypt

Journal of Saudi Chemical Society (2022) **26**, 101508

King Saud University

Journal of Saudi Chemical Society

www.ksu.edu.sa
www.sciencedirect.com

ORIGINAL ARTICLE

Augmented formic acid electro-oxidation at a co-electrodeposited Pd/Au nanoparticle catalyst

Yaser M. Asal [a], **Ahmad M. Mohammad** [b,*], **Sayed S. Abd El Rehim** [c], **Islam M. Al-Akraa** [a,*]

[a] *Department of Chemical Engineering, Faculty of Engineering, The British University in Egypt, Cairo 11837, Egypt*
[b] *Chemistry Department, Faculty of Science, Cairo University, Cairo 12613, Egypt*
[c] *Chemistry Department, Faculty of Science, Ain Shams University, 11566 Abbassia, Cairo, Egypt*

Received 23 March 2022; revised 28 May 2022; accepted 6 June 2022
Available online 9 June 2022

KEYWORDS

Pd-Au;
Co-electrodeposition;
Fuel Cells;
Formic acid oxidation;
Poisoning

Abstract In this study, the formic acid electro-oxidation reaction (FAEOR) was catalyzed on a Pd-Au co-electrodeposited binary catalyst. The kinetics of FAEOR were intensively impacted by changing the Pd^{2+}:Au^{3+} molar ratio in the deposition medium. The Pd_1-Au_1 catalyst (for which the Pd^{2+}:Au^{3+} molar ratio was 1:1) acquired the highest activity with a peak current density for the direct FAEOR (I_p) of 4.14 mA cm^{-2} (ca. 13- times higher than that (ca. 0.33 mA cm^{-2}) of the pristine Pd_1-Au_0 catalyst). It also retained the highest stability that was denoted in fulfilling ca. 0.292 mA cm^{-2} (ca. 19-times higher than 0.015 mA cm^{-2} of the pristine Pd_1-Au_0 catalyst) after 3600 s of continuous electrolysis at 0.05 V. The CO stripping and impedance measurements confirmed, respectively, the geometrical and electronic enhancements in the proposed catalyst.

1. Introduction

"Together for our planet" was the motto of the UN climate change conference (COP26) in UK which highlighted the urgency to sustain a greener, more resilient future for us all. Due to the overwhelming increase in the continuous combustion of traditional fossil fuels, a pronounced growth was observed in the concentration of greenhouse gases (GHGs) that can badly affect our ecosystem. These included carbon dioxide (CO_2, whose atmospheric level approached ca. 415 ppm; surpassing approximately twice earlier readings) [1], methane (CH_4), ozone (O_3), nitrous oxide (N_2O), water vapour, and some synthetic chemicals as chlorofluorocarbons (CFCs) [2]. Hence, most of recent studies aimed to explore reliable, clean (minimum GHGs), efficient, and sustainable technologies for transportation, electricity production, and many other vital applications [3–13].

In this context, the liquid fuel cells (LFCs) that worked with the electrochemical combustion of liquid fuels as ethanol [14], ethylene glycol [15], methanol [16], and formic acid (FA) [17–19], in a better, safer and more convenient scenario than

* Corresponding authors.
E-mail addresses: yasser.mohamed@bue.edu.eg (Y.M. Asal), ammohammad@cu.edu.eg (A.M. Mohammad), islam.ahmed@bue.edu.eg (I.M. Al-Akraa).
Peer review under responsibility of King Saud University.

Production and hosting by Elsevier

https://doi.org/10.1016/j.jscs.2022.101508

H_2 appeared promising for multiple portable and stationary applications with high conversion efficiencies and low operating temperatures [20,21].

Of these LFCs, the direct formic acid FCs (DFAFCs) owned a high (1750 kW h L^{-1}) energy density [22], large theoretical open-circuit potential (~1.40 V) [23,24], and rapid oxidation kinetics beside using a non-flammable (8.4–100.8 °C) and non-toxic fuel (FA) of least (relative to methanol and many other liquid fuels) crossover through the Nafion® membrane; the cell electrolyte [25–27]. Yet, it remained unprepared for commercialization until exploring a cheap, efficient, and stable anodic catalyst for the formic acid electro-oxidation reaction (FAEOR); the main anodic reaction in DFAFCs.

Till now, the most proper anodic catalysts for DFAFCs are either Pt or Pd-based. But, the high cost, limited supply, and high poisoning level of Pt-based catalysts encountered their large-scale industrial applications for DFAFCs [28–34]. That drove attention to Pd for its wider availability, lower price, similar geometric structure, and lower poisoning [35–42]. Nevertheless, Pd-based catalysts experienced a critical rapid diminution of catalytic performance over long periods of electrolysis which was sometimes attributed to a mechanical detachment of Pd in highly acidic solutions and/or adsorption of poisonous oxidation intermediates such as carbon monoxide (CO) at its surfaces [43–45].

One way to overcome this deterioration in the catalytic performance of Pd catalysts employed blending Pd with other metals such as gold [46], ruthenium [47], iron [48], cobalt [49] and nickel [50] and/or metal oxide as nickel oxide [51,52] and manganese oxide [51]. This could amend the Pd surface against poisoning and could further enhance its mechanical stability.

According to the "d-band center theory", alloying Pd with other metals can modulate its electronic structure [38,53] that alters the adsorption tendency for a given species [38]. For example, the modification of Pd with Au succeeded not only to increase the catalyst's resistance to CO poisoning but also to increase the catalyst's durability in harsh experimental conditions [38]. In view of this interesting catalytic performance, the Pd-Au catalyst appeared attractive. We, herein, propose the fabrication of a Pd-Au co-electrodeposited catalyst onto a glassy carbon (GC) substrate for propitious FAEOR. The "simultaneous co-electrodeposition" protocol that was adopted for the catalyst's preparation ensured a fast and simple nanoparticles loading with a convenient homogeneity of the catalytic constituents that were added in minute loadings [23,54]. The role of mixing different Pd^{2+}:Au^{3+} molar ratios in the deposition medium on the catalyst's performance toward FAEOR was examined. Several characterization tools were utilized to assess the catalytic performance of the investigated catalyst and to elucidate the reaction mechanism.

2. Experimental

2.1. Materials and reagents

Palladium (II) acetate ($Pd(CH_3COO)_2$, trimer, Pd 45.9–48.4%, hydrogen tetrachloroaurate (III) trihydrate ($HAuCl_4{\cdot}3H_2O$, 99.99% metals basis, Au 49.0%), Pellets of sodium hydroxide (NaOH), anhydrous sodium sulfate (Na_2SO_4), sulphuric acid (AR, H_2SO_4, 98%) and formic acid (FA, HCOOH, 98%)) received from Sigma Aldrich and Alfa Aesar.

2.2. Instruments and electrodes

The surface of the proposed catalysts was morphologically and compositionally characterized using a field emission scanning electron microscope (FE-SEM, Quattro S, Thermo Fisher Scientific USA equipped with AMETEK USA Element Detector) and the associated energy dispersive X-ray spectroscope (EDS), respectively. An X-Ray Diffractometer (XRD, PANalytical X'Pert Pro powder) of a high resolution that operated with a Cu anode at 154 μm was utilized to explore the crystallography of the proposed catalysts. A Bio-Logic SAS (model SP-150) Potentiostat operated with EC-Lab software was utilized in the electrochemical measurements in a three-electrode system including, respectively, a GC (d = 5 mm with 0.196 cm^2 geometric area), spiral Pt wire, and an Ag/AgCl/NaCl (3 M) as the working, counter and reference electrodes. All these electrodes were purchased from ALS Japan. Currents were normalized relative to the electrochemical surface area (ECSA) of Pd (A_{pd}) of each catalyst (Fig. S1) which was calculated from the charge (Q_{Pd} (μC)) consumed in the PdO → Pd reduction in the cyclic voltammogram of each catalyst in 0.5 M H_2SO_4 (see later Fig. 1) using this assumption: $A_{Pd}(cm^2) = \frac{Q_{Pd}\ (\mu C)}{420\ (\mu C\ cm^{-2})}$ [55].

2.3. Fabrication of catalysts

The catalysts were fabricated by a "simultaneous co-electrodeposition" technique as previously explained [56,57]. Ahead of deposition, a GC substrate was mechanically polished with No. 2000 emery paper before a further polishing on a polishing microcloth with aqueous slurries of successively finer alumina powder (down to 0.06 mm). Next, the GC electrode was rinsed thoroughly with secondly distilled water [58]). The catalyst's fabrication involved the potentiostatic electrodeposition of Pd and Au onto a clean GC surface at −0.2 V (for 10 mC) in 2.0 mM $Pd(CH_3COO)_2$ and 2.0 mM $HAuCl_4{\cdot}3H_2O$ aqueous solution in 0.1 M Na_2SO_4. Proper abbreviations were

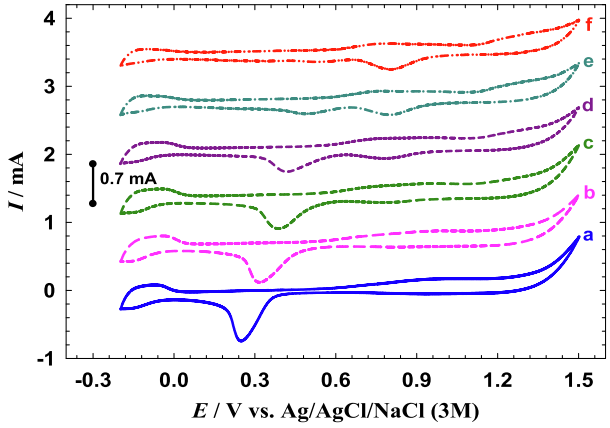

Fig. 1 CVs measured in 0.5 M H_2SO_4 at potential scan rate of 100 mV s^{-1} for the Pd_1-Au_0, Pd_1-$Au_{0.2}$, Pd_1-$Au_{0.4}$, Pd_1-$Au_{0.6}$, Pd_1-$Au_{0.8}$, and Pd_1-Au_1 (a-f, respectively) modified catalysts.

assigned to the different catalysts based on the Pd^{2+} and Au^{3+} molar ratios in the deposition medium. For examples, the Pd_1-Au_0 and Pd_1-Au_1 catalysts denoted the existence of Pd^{2+} and Au^{3+} in the deposition mediums in molar ratios of 1:0 and 1:1, respectively.

3. Results and discussion

3.1. Electrochemical characterizations

To accurately explore the surface composition of the catalyst's ingredients, cyclic voltammetry (CV) experiments were performed. Fig. 1 represents the CVs measured in aqueous solution of 0.5 M H_2SO_4 for the Pd_1-Au_0, Pd_1-$Au_{0.2}$, Pd_1-$Au_{0.4}$, Pd_1-$Au_{0.6}$, Pd_1-$Au_{0.8}$, and Pd_1-Au_1 (Fig. 1a-f, respectively) catalysts in a potential range between −0.2 and +1.5 V at a potential scan rate of 100 mV s^{-1}. Fig. 1a (Pd_1-Au_0 catalyst) displays the characteristic behavior of Pd surface [59,60], in which the adsorption–desorption ($H_{ads\text{-}des}$) peaks of hydrogen between −0.2 and 0.0 V, the Pd oxidation (Pd → PdO) extending from ca. 0.6 to 1.5 V, and the PdO reduction (PdO → Pd) at ca. 0.24 V appeared obviously.

Interestingly, for the Pd_1-$Au_{0.2}$ (Fig. 1b) to Pd_1-Au_1 (Fig. 1f) catalysts, the following remarks were observed and data were summarized in Table 1:

- The peak current intensities of the $H_{ads\text{-}des}$ and PdO → Pd decreased systematically. As the same charge employed for the Pd deposition in the Pd_1Au_0 catalyst was used for the simultaneous deposition of both Pd and Au in other catalysts (Fig. 1b-f), the decrease of these peak heights was plausible.
- A new weak oxidation peak was observed at ca. 1.35 V corresponding to the Au → AuO oxidation [54]. Its subsequent reduction (AuO → Au) was more obvious (particularly for the catalysts of high Au loading) at ca. 0.8 V (the typical characteristic features of Au in the Pd_0-Au_1 catalyst appear in Fig. S2A) [54]. The weakness of the Au → AuO oxidation peak might be understood in view of the possible interference with the Pd → PdO oxidation peak. This might provide an evidence for the successful deposition of Au along with Pd at the GC surface.
- A positive shift (relatively to the Pd_1-Au_0 catalyst) was observed in the potential of PdO → Pd peak, and this shift was gradually increased from Pd_1-$Au_{0.2}$ (Fig. 1b) to Pd_1-Au_1 (Fig. 1f) catalysts. This can possibly infer an electronic and/or a compositional change of the Pd surface that can originate from the interaction with Au. This behavior was observed previously for Ir-modified Pd catalysts [61].

Table 1 Real surface area of Pd (A_{Pd}) and Au (A_{Au}) as extracted from Fig. 1.

Catalyst	A_{Pd} (cm^2)	A_{Au} (cm^2)
Pd_1-Au_0	1.74	0.00
Pd_1-$Au_{0.2}$	1.55	0.01
Pd_1-$Au_{0.4}$	1.28	0.10
Pd_1-$Au_{0.6}$	0.85	0.28
Pd_1-$Au_{0.8}$	0.31	0.47
Pd_1-Au_1	0.07	0.58

A_{Pd}: real area of Pd, A_{Au}: real area of Au.

3.2. Materials characterization

Fig. 2 shows the FE-SEM micrographs of the Pd_1-Au_0, Pd_1-$Au_{0.2}$, Pd_1-$Au_{0.4}$, Pd_1-$Au_{0.6}$, Pd_1-$Au_{0.8}$, and Pd_1-Au_1 (Fig. 2-A-F, respectively) catalysts and the insets show the corresponding particle size distribution (adopted by ImageJ software). Fig. 2A (Pd_1-Au_0 catalyst) displays the deposition of Pd onto the GC surface in well-distributed spherical particles with an average particle size of ca. 150 nm. The Pd_1-$Au_{0.2}$ catalyst (Fig. 2B) retained the same spherical shape but in a larger particle size (ca. 178 nm). The same trend of increasing the average particle size continued for the Pd_1-$Au_{0.4}$, Pd_1-$Au_{0.6}$, Pd_1-$Au_{0.8}$, and Pd_1-Au_1 catalysts (Fig. 2C-F), but with a systematic decrease in the particle's coverage. The average particle size of the Pd_1-Au_1 catalyst was ca. 390 nm. The FE-SEM investigation agreed with the electrochemical characterization in lowering the Pd surface area with Au content in the deposition medium; possibly, inferring the successful deposition of Au with Pd. Nothing indicated the separation of Pd and Au particles and this might recommend a possible blending/alloying.

To ensure the successful co-electrodeposition of Pd and Au onto the GC surface, analysis with energy dispersive X-ray spectroscopy (EDS) was performed for the Pd_1-Au_0, Pd_1-$Au_{0.2}$, Pd_1-$Au_{0.4}$, Pd_1-$Au_{0.6}$, Pd_1-$Au_{0.8}$, and Pd_1-Au_1 catalysts (Fig. 3a-f, respectively). All catalysts showed the relative peaks related to their composition (C, O, Pd for all catalysts (Fig. 3a-f) in addition to Au for the Au-modified catalysts (Fig. 3b-f)) at their standard positions [56,62]. This confirmed the simultaneous electrodeposition of Pd and Au at the GC surface. Furthermore, the elemental mapping of the Pd_1-Au_0 and Pd_1-Au_1 catalysts reflected the good distribution of all elements, as Fig. S3 shows.

Additionally, XRD was employed to examine the crystallography of the Pd_1-Au_0, Pd_1-$Au_{0.2}$, Pd_1-$Au_{0.4}$, Pd_1-$Au_{0.6}$, Pd_1-$Au_{0.8}$, and Pd_1-Au_1 catalysts (Fig. 4a-f, respectively). The C (002) and C (100) diffraction peaks were observed at ca. 25.2° and 43.1°, respectively (JCPDS card No. 075-1621) [63]. While, the Pd (111), Pd (200), Pd (220), and Pd (311) diffraction peaks were identified, respectively, at ca. 38.3°, 44.5°, 65.1°, and 78.3° (JCPDS card No. 96-101-1105) [55,60,64]. On the other side, Fig. S2B shows the XRD pattern of the Pd_0-Au_1 catalyst where all Au diffraction peaks were identified at their reference positions (JCPDS card No. 96-901-1613). Remarkably in Fig. 4b-f (binary catalysts), the peaks of Au and Pd, which very close to each other (see Fig. 4a and S2B), overlapped together with an observable increase in the peaks' intensities.

3.3. FAEOR: electro-catalytic activity and stability

As previously described, FAEOR proceeds at Pd-based catalysts mainly via the dehydrogenation pathway (Eq. (1)) that includes the direct oxidation of FA to CO_2 with a little bit contribution of Pd poisoning by CO intermediate (Eq. (2)) that would be further oxidized (Eq. (4)) at higher potentials after the Pd surface hydroxylation (Eq. (3)) [65,66].

$$HCOOH + Pd \rightarrow Pd + CO_2 + 2H^+ + 2e^- \quad (1)$$

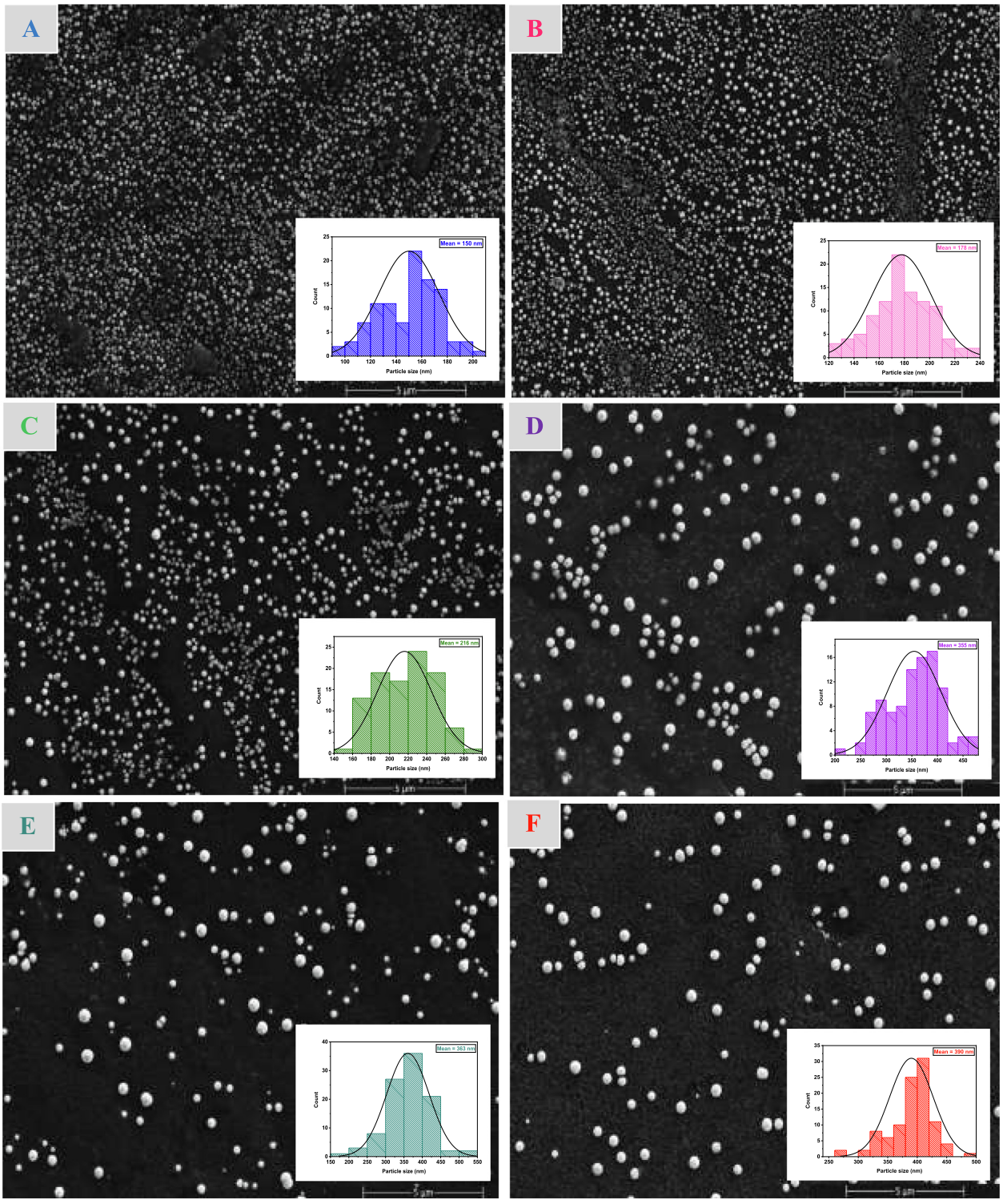

Fig. 2 SEM micrographs the Pd_1-Au_0, Pd_1-$Au_{0.2}$, Pd_1-$Au_{0.4}$, Pd_1-$Au_{0.6}$, Pd_1-$Au_{0.8}$, and Pd_1-Au_1 (A-F, respectively) catalysts. The insets show the particle size distribution of each catalyst.

$$HCOOH + Pd \rightarrow Pd - CO + H_2O \quad (2)$$

$$Pd + H_2O \rightarrow Pd - OH + H^+ + e^- \quad (3)$$

$$Pd - CO + Pd - OH \rightarrow 2Pd + CO_2 + H^+ + e^- \quad (4)$$

Fig. 5 displays the CVs of FAEOR at the Pd_1-Au_0, Pd_1-$Au_{0.2}$, Pd_1-$Au_{0.4}$, Pd_1-$Au_{0.6}$, Pd_1-$Au_{0.8}$, and Pd_1-Au_1 (a-f, respectively) catalysts measured at a potential scan rate of 100 mVs^{-1} in 0.3 M FA aqueous solution having a pH of 3.5. This pH value was adjusted by the addition of an appro-

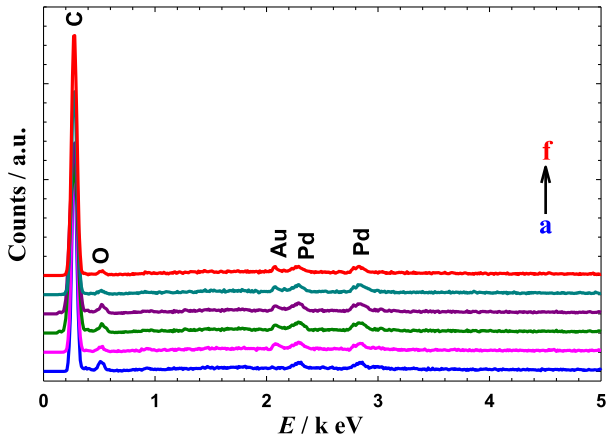

Fig. 3 EDS spectra of the Pd_1-Au_0, Pd_1-$Au_{0.2}$, Pd_1-$Au_{0.4}$, Pd_1-$Au_{0.6}$, Pd_1-$Au_{0.8}$, and Pd_1-Au_1 catalysts (a-f, respectively).

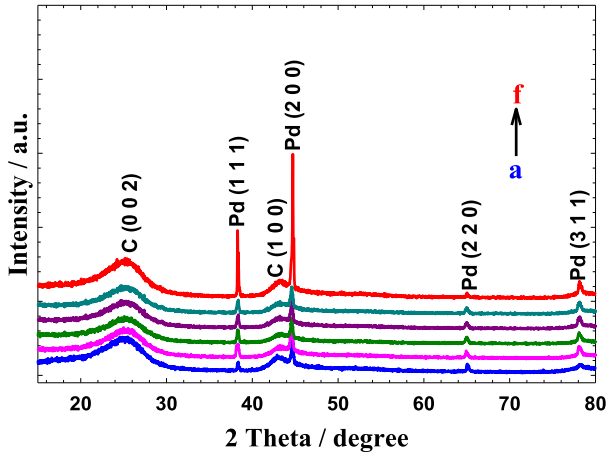

Fig. 4 XRD patterns of the Pd_1-Au_0, Pd_1-$Au_{0.2}$, Pd_1-$Au_{0.4}$, Pd_1-$Au_{0.6}$, Pd_1-$Au_{0.8}$, and Pd_1-Au_1 catalysts (a-f, respectively).

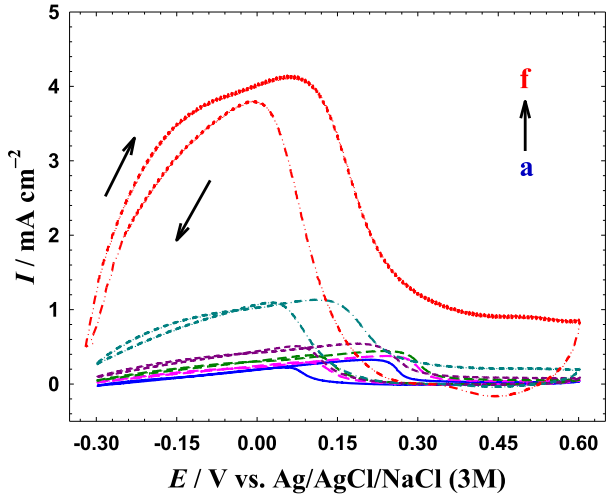

Fig. 5 CVs of FAEOR measured in 0.3 M FA (pH = 3.5) at a potential scan rate of 100 mV s^{-1} for the Pd_1-Au_0, Pd_1-$Au_{0.2}$, Pd_1-$Au_{0.4}$, Pd_1-$Au_{0.6}$, Pd_1-$Au_{0.8}$, and Pd_1-Au_1 (a-f, respectively) catalysts.

priate amount of sodium hydroxide. Fig. 5a (blue curve) displays the FAEOR at the unmodified Pd catalyst (Pd_1-Au_0 catalyst). In the forward scan, a single oxidation peak appeared at ca. 0.21 V with ca. 0.33 mA cm^{-2}. This peak was assigned to the direct oxidation of FA to CO_2, as discussed above. The current density and the potential of the oxidation peak will be denoted respectively as I_p and E_p. With the increase of Au (which is inactive for FAEOR (see Fig. S4)) in the catalyst (Fig. 5b-f), a systematic increase in I_p was observed; reaching ca. 4.14 mA cm^{-2} at the Pd_1-Au_1 catalyst (more than 13 times compared to the corresponding value obtained at the Pd_1-Au_0 catalyst). This was coupled with ca. −0.14 V shift in the onset potential (E_p) of the direct FAEOR. All values of I_p, E_p, and enhancement factor for all catalysts are given in Table 2 which demonstrated the superiority (enhanced catalytic activity) of Au-containing Pd catalysts for FAEOR. Interestingly, Table S1 showed that the activity of the Pd_1-Au_1 catalyst toward FAEOR was higher than many of those observed previously. Moreover, Fig. S5 and Table S2 showed the privilege of using the simultaneous co-electrodeposition over the sequential methodology in terms of getting a higher I_p and a lower E_p for FAEOR.

Moreover, the turnover number (TON, the number of FA molecules oxidized at a certain potential (0.05 V) per second and per catalytic active site was calculated to probe the specific electrocatalytic ability of the catalyst as follows [67,68]:

$$TON = \frac{I_{0.05V}}{2 \times Q_{pd}} \quad (5)$$

where, Q_{Pd} is the charge density calculated from the Pd-oxide reduction peak and all the electroactive sites of Pd are considered in the TON calculation.

TON for FAEOR at the Pd_1-Au_1 catalyst was 5 s^{-1}, which is ca. 18 times of that calculated at the Pd_1-Au_0 catalyst (see the corresponding values for all catalysts in Table 2). This again supported the promising candidacy of the proposed Pd_1-Au_1 catalyst for FAEOR.

Stabilities of the investigated catalysts were inspected during prolonged electrolysis. Chronoamperometric (*i-t*) measurements were employed for all proposed catalysts at 0.05 V with a continuous electrolysis for 3600 s. It is important to highlight that the poor stability of the Pd-based catalysts is one of the core challenges in DFAFCs and this was attributed to a possible poisoning by oxidation products during FAEOR, the mechanical split up, and/or the chemical dissolution of Pd during continuous electrolysis [59,69,70]. This was observed

Table 2 A summary of electro-catalytic data (I_p and E_p) obtained as a function of the Pd/Au molar ratio. Data were extracted from Fig. 5.

Catalyst	I_p/mA cm^{-2}	Enhancement Factor*	E_p/V	TON/s^{-1}
Pd_1-Au_0	0.33	–	0.21	0.27
Pd_1-$Au_{0.2}$	0.38	1.15	0.24	0.31
Pd_1-$Au_{0.4}$	0.45	1.36	0.24	0.38
Pd_1-$Au_{0.6}$	0.55	1.67	0.19	0.54
Pd_1-$Au_{0.8}$	1.14	3.45	0.11	1.30
Pd_1-Au_1	4.14	12.5	0.07	5.00

* Enhancement Factor = $\frac{\text{Ip modified Pd–Au catalyst}}{\text{Ip unmodified Pd catalyst}}$.

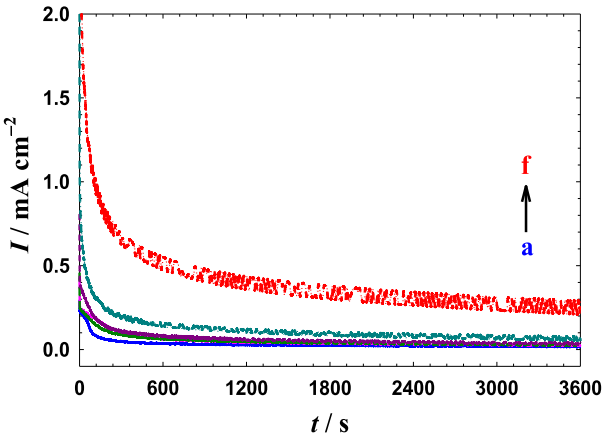

Fig. 6 Current transients obtained at 0.05 V during FAEOR in 0.3 M FA (pH = 3.5) at the Pd_1-Au_0, Pd_1-$Au_{0.2}$, Pd_1-$Au_{0.4}$, Pd_1-$Au_{0.6}$, Pd_1-$Au_{0.8}$, and Pd_1-Au_1 (a-f, respectively) catalysts.

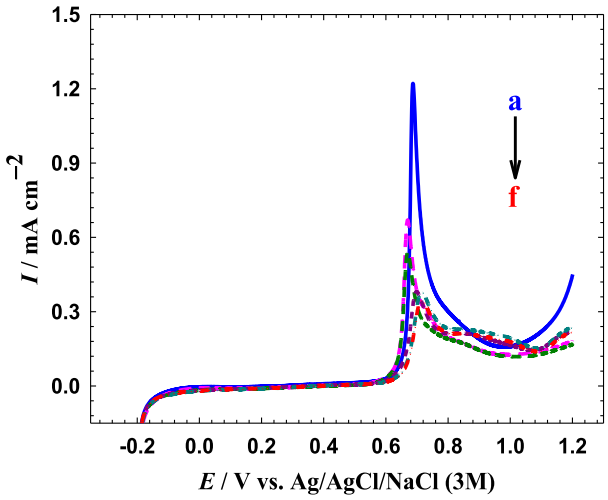

Fig. 7 LSVs measured at a potential scan rate of 20 mVs^{-1} in 0.5 M Na_2SO_4 (pH = 3.5) for the oxidative CO stripping obtained at the Pd_1-Au_0, Pd_1-$Au_{0.2}$, Pd_1-$Au_{0.4}$, Pd_1-$Au_{0.6}$, Pd_1-$Au_{0.8}$, and Pd_1-Au_1 (a-f, respectively) catalysts. Before measurements, CO was adsorbed from 0.5 M FA at the open circuit potential for 20 min.

clearly at the Pd_1-Au_0 catalyst (Fig. 6a). The Au-modified Pd catalysts (Fig. 6b-f) exhibited higher current densities and lower poisoning rates. The Pd_1-Au_1 catalyst showed the highest stability reaching ca. 0.292 mA cm^{-2} (ca. 19 times higher) after 3600 s of electrolysis compared to ca. 0.015 mA cm^{-2} that obtained at the Pd_1-Au_0 catalyst. Moreover, the CV measured in Fig. 1 was repeated again for the Pd_1-Au_0 and the Pd_1-Au_1 catalysts after the long-term experiment in Fig. 6 and the losses in the A_{Pd} were 25 and 19 %, respectively from their initial values in Table 1. This reflected the vital effect of Au in enhancing the stability of the proposed catalysts. The question now is how could Au boost the catalytic performance of the proposed catalysts? This will be elaborated in the following section.

3.4. Mechanisms of enhancement: CO stripping and impedance measurements

To precisely determine the catalytic role of Au in the proposed catalysts, CO was permitted to chemisorb at open circuit potentials from 0.5 M FA onto the Pd_1-Au_0, Pd_1-$Au_{0.2}$, Pd_1-$Au_{0.4}$, Pd_1-$Au_{0.6}$, Pd_1-$Au_{0.8}$, and Pd_1-Au_1 catalysts for 20 min then oxidatively stripped in 0.5 M Na_2SO_4 (pH = 3.5) as shown in Fig. 7a-f, respectively. The Pd_1-Au_0 catalyst (Fig. 7a) showed a large oxidation peak at ca. 0.68 V. The peak charge that was related to the amount of adsorbed CO (Q_{CO}) was ca. 0.52 mC. This behavior was related to the Pd surface blocking by the CO intermediate that got oxidatively desorbed at 0.68 V [62]. By increasing the Au: Pd ratio in the deposition medium (Fig. 7b-f, respectively), a systematic shrinkage in the CO oxidation charge was observed reaching ca. 0.21 mC at the Pd_1-Au_1 catalyst. Table 3 shows the values of Q_{CO} for all proposed catalysts. Such a decrease in the poisoning impact was related to the third body effect that showed the important role of Au in interrupting the contiguity of Pd atoms required for CO adsorption [71]. Two more observations were noticed after a deeper inspection of Fig. 7; the other peak observed around 1 V was related to either oxidation of CO at different facets [72], at different surfaces (single Pd or PdAu intermetallics) [73], or to the oxidation of other CO-like intermediates [71]. Additionally, a small shift (±0.02 V) in the CO oxidation peak was observed at all Au-modified catalysts. This shift was thought to originate from electronic modification of Pd surface (in agreement with the previous elucidations) [71,74].

From another side, the charge transfer kinetics was evaluated using the electrochemical impedance spectroscopy (EIS). Fig. 8 displays the Nyquist plots measured at open circuit potential between 10 mHz and 100 kHz in 0.3 M FA solution having a pH of 3.5. The data fitting was conducted with the aid of the EC-Lab software and the inset of Fig. 8 shows this equivalent circuit.

Over there, R_s, R_{ct}, and C_{dl} referred respectively to the solution resistance, charge transfer resistance, and double layer capacitance of the electrochemical system. The semicircular diameter of a Nyquist plot corresponds to R_{ct} of the reaction at this particular catalyst [75]. Fig. 8a (Pd_1-Au_0 catalyst) depicted a large semicircular diameter, i.e., large R_{ct} value (0.9 kΩ) that reflected the slow oxidation kinetics and the catalyst's poisoning. Interestingly, at all Au-modified catalysts (Fig. 8b-f), the R_{ct} decreased in a trend reaching 0.24 kΩ for the Pd_1-Au_1 catalyst. Such a decrease in R_{ct} at the Au-modified catalysts was thought to originate from an electronic effect that could facilitate the charge transfer kinetics during

Table 3 A summary of the poisoning degree (Q_{CO}) obtained as a function of the Pd/Au molar ratio. Data were extracted from Fig. 7.

Catalyst	Q_{CO} (mC)
Pd_1-Au_0	0.52
Pd_1-$Au_{0.2}$	0.47
Pd_1-$Au_{0.4}$	0.36
Pd_1-$Au_{0.6}$	0.31
Pd_1-$Au_{0.8}$	0.29
Pd_1-Au_1	0.21

Table 4 A summary of the Nyquist plot data (R_s, R_{ct} and i_0) obtained as a function of the Pd/Au molar ratio. Data were extracted from Fig. 8.

Catalyst	R_s (kΩ)	$R_s + R_{ct}$ (kΩ)	R_{ct} (kΩ)	i_o/A cm^{-2}
Pd_1-Au_0	0.26	1.16	0.90	2.85×10^{-5}
Pd_1-$Au_{0.2}$	0.23	0.51	0.28	9.17×10^{-5}
Pd_1-$Au_{0.4}$	0.23	0.51	0.28	9.17×10^{-5}
Pd_1-$Au_{0.6}$	0.22	0.48	0.26	9.88×10^{-5}
Pd_1-$Au_{0.8}$	0.24	0.51	0.27	9.51×10^{-5}
Pd_1-Au_1	0.22	0.47	0.24	1.07×10^{-4}

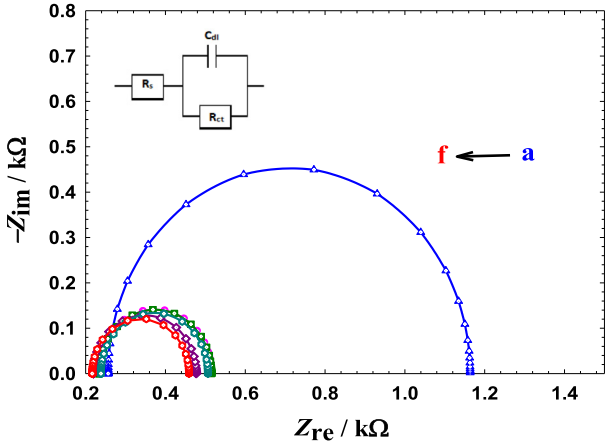

Fig. 8 Nyquist plots obtained at the Pd_1-Au_0, Pd_1-$Au_{0.2}$, Pd_1-$Au_{0.4}$, Pd_1-$Au_{0.6}$, Pd_1-$Au_{0.8}$, and Pd_1-Au_1 (a-f, respectively) catalysts in aqueous solution of 0.3 M FA (pH = 3.5). The AC potential amplitude was recorded at the open circuit potential (OCP) and the frequency range from 10 mHz to 100 kHz. The inset depicts the recommended equivalent circuit for the electrochemical setup.

FAEOR [71,74]. Table 4 summarizes the R_{ct} values of all modified catalysts. Additionally, the standard exchange current density (i_o) can be used to monitor the intrinsic catalytic activity of our proposed catalysts. A larger i_o reflects a higher electrocatalytic activity toward FAEOR. This can be calculated utilizing the R_{ct} according to the following equation [76,77]:

$$i_o = \frac{R \times T}{F \times R_{ct}} \quad (6)$$

where R, T and F are gas constant, absolute temperature, and Faradic constant, respectively. The calculated i_o values were listed in Table 4 where the Pd_1-Au_1 catalyst acquired the highest value (1.07×10^{-4} A cm^{-2}) which was ca. 4 times higher than that of the Pd_1-Au_0 catalyst (2.85×10^{-5} A cm^{-2}); proving that the Pd_1-Au_1 catalyst has a better intrinsic electrocatalytic activity. The CO stripping and impedance measurements assigned both of the third body and electronic effects for the catalytic role of Au in the Au-modified Pd catalysts.

4. Conclusion

An innovative Pd-Au co-electrodeposited binary catalyst was fabricated onto the GC substrate and its catalytic activity was further investigated toward FAEOR. The relative Pd^{2+}: Au^{3+} ratio in the deposition medium impacted, to a great extent, the catalytic activity and stability toward FAEOR. After careful inspection, the Pd_1-Au_1 catalyst showed the highest catalytic activity (4.14 mA cm^{-2} compared to 0.33 mA cm^{-2} obtained at the Pd_1-Au_0 catalyst) and stability (19 times higher current density after 3600 s of continuous electrolysis compared with the Pd_1-Au_0 catalyst) toward FAEOR. The CO stripping and impedance measurements confirmed both the third body and the electronic effects as the mechanisms of catalytic enhancement.

CRediT authorship contribution statement

Yaser M. Asal: Methodology, Investigation, Writing - Original draft. **Ahmad M. Mohammad:** Conceptualization, Investigation, Writing- review & editing. **Sayed S. Abd El Rehim:** Supervision. **Islam M. Al-Akraa:** Conceptualization, Supervision, Methodology, Investigation, Formal analysis, Writing- review & editing.

Declaration of Competing Interest

The authors declare that they have no known competing financial interests or personal relationships that could have appeared to influence the work reported in this paper.

Appendix A. Supplementary data

Supplementary data to this article can be found online at https://doi.org/10.1016/j.jscs.2022.101508.

References

[1] R. Sun, Y. Liao, S.-T. Bai, M. Zheng, C. Zhou, T. Zhang, Heterogeneous catalysts for CO2 hydrogenation to formic acid/formate: from nanoscale to single atom, Energy Environ. Sci. 14 (2021) 1247–1285.
[2] D.U. Nielsen, X.-M. Hu, K. Daasbjerg, T. Skrydstrup, Chemically and electrochemically catalysed conversion of CO2 to CO with follow-up utilization to value-added chemicals, Nat. Catal. 1 (4) (2018) 244–254.
[3] X.-Y. Wang, Z. Han, J.-J. Duan, J.-J. Feng, H. Huang, A.-J. Wang, Facile construction of 3D hyperbranched PtRh nanoassemblies: A bifunctional electrocatalyst for hydrogen evolution and polyhydric alcohol oxidation reactions, Int. J. Hydrog. Energy 45 (2020) 8433–8443.
[4] J.H. Montoya, L.C. Seitz, P. Chakthranont, A. Vojvodic, T.F. Jaramillo, J.K. Nørskov, Materials for solar fuels and chemicals, Nat. Mater. 16 (1) (2017) 70–81.
[5] M.E. Scofield, H. Liu, S.S. Wong, A concise guide to sustainable PEMFCs: recent advances in improving both oxygen reduction catalysts and proton exchange membranes, Chem. Soc. Rev. 44 (2015) 5836–5860.
[6] M.S. Faber, S. Jin, Earth-abundant inorganic electrocatalysts and their nanostructures for energy conversion applications, Energy Environ Sci. 7 (11) (2014) 3519–3542.
[7] K. Stangeland, H.H. Navarro, H.L. Huynh, W.M. Tucho, Z. Yu, Tuning the interfacial sites between copper and metal oxides (Zn, Zr, In) for CO2 hydrogenation to methanol, Chem. Eng. Sci. 238 (2021) 116603.
[8] V.G. Dileepkumar, K.R. Balaji, R. Vishwanatha, B.M. Basavaraja, S. Ashoka, I. M. Al-Akraa, M.S. Santosh, S.

Rtimi, Sami Rtimi, CoSe2 grafted on 2D gC3N4: A promising material for wastewater treatment, electrocatalysis and energy storage, Chem. Eng. J. 446 (2022) 137023.
[9] I.M. Al-Akraa, T. Ohsaka, A.M. Mohammad, A promising amendment for water splitters: Boosted oxygen evolution at a platinum, titanium oxide and manganese oxide hybrid catalyst, Arab. J. Chem. 12 (2019) 897–907.
[10] I.M. Al-Akraa, Y.M. Asal, S.D. Khamis, Assembling of NiOx/MWCNTs-GC anodic nanocatalyst for water electrolysis applications, Int. J. Electrochem. Sci. 13 (2018) 9712–9720.
[11] I.M. Al-Akraa, A.M. Mohammad, M.S. El-Deab, B.E. El-Anadouli, Flower-shaped gold nanoparticles: Preparation, characterization, and electrocatalytic application, Arab. J. Chem. 10 (2017) 877–884.
[12] I.M. Al-Akraa, A.M. Mohammad, M.S. El-Deab, B.E. El-Anadouli, Self-assembling of gold nanoparticles array for electro-sensing applications, Int. J. Electrochem. Sci. 8 (2013) 458–466.
[13] A.M. Mohammad, S. Dey, K.K. Lew, J.M. Redwing, S.E. Mohney, Fabrication of Cobalt Silicide Nanowire Contacts to Silicon Nanowires, J. Electrochem.Soc. 150 (2003) G577-G580.
[14] O. Sahin, D. Duzenli, H. Kivrak, An ethanol electrooxidation study on carbon-supported Pt-Ru nanoparticles for direct ethanol fuel cells, Energy Sources 38 (2016) 628–634.
[15] B. Ulas, A. Caglar, A. Kivrak, H. Kivrak, Atomic molar ratio optimization of carbon nanotube supported PdAuCo catalysts for ethylene glycol and methanol electrooxidation in alkaline media, Chem. Pap. 73 (2) (2019) 425–434.
[16] H. Kivrak, M. Can, H. Duru, O. Sahin, Methanol electrooxidation study on mesoporous silica supported Pt–Co direct methanol fuel cell anode, Int. J. Chem. React. Eng. 12 (2014) 369–375.
[17] B. Ulas, A. Kivrak, N. Aktas, H. Kivrak, Carbon monoxide and formic acid electrooxidation study on Au decorated Pd catalysts prepared via microwave assisted polyol method, Fullerenes, Fuller. Nanotub. Carbon Nanostruct. 27 (7) (2019) 545–552.
[18] Y. Karatas, A. Bulut, M. Yurderi, I.E. Ertas, O. Alal, M. Gulcan, PdAu-MnOx nanoparticles supported on amine-functionalized SiO2 for the room temperature dehydrogenation of formic acid in the absence of additives, Appl. Catal. B: Environ. 180 (2016) 586–595.
[19] I.M. Al-Akraa, Y.M. Asal, A.M. Mohammad, Surface engineering of Pt surfaces with Au and cobalt oxide nanostructures for enhanced formic acid electro-oxidation, Arab. J. Chem.103965 15 (2022).
[20] X. Chen, G. Wu, J. Chen, X. Chen, Z. Xie, X. Wang, Synthesis of "clean" and well-dispersive Pd nanoparticles with excellent electrocatalytic property on graphene oxide, J. Am. Chem. Soc. 133 (11) (2011) 3693–3695.
[21] P. Strasser, S. Koh, T. Anniyev, J. Greeley, K. More, C. Yu, Z. Liu, S. Kaya, D. Nordlund, H. Ogasawara, M.F. Toney, A. Nilsson, Lattice-strain control of the activity in dealloyed core-shell fuel cell catalysts, Nat Chem. 2 (6) (2010) 454–460.
[22] B.C. Ong, S.K. Kamarudin, S. Basri, Direct liquid fuel cells: A review, Int. J. Hydrog. Energy 42 (15) (2017) 10142–10157.
[23] Y.M. Asal, I.M. Al-Akraa, A.M. Mohammad, M.S. El-Deab, A competent simultaneously co-electrodeposited Pt-MnOx nanocatalyst for enhanced formic acid electro-oxidation, J. Taiwan Inst. Chem. Eng. 96 (2019) 169–175.
[24] I.M. Al-Akraa, A.E. Salama, Y.M. Asal, A.M. Mohammad, Boosted performance of NiOx/Pt nanocatalyst for the electro-oxidation of formic acid: A substrate's functionalization with multi-walled carbon nanotubes, Arab. J. Chem. 14 (2021) 103383.
[25] M. Marinšek, M. Šala, B. Jančar, A study towards superior carbon nanotubes-supported Pd-based catalysts for formic acid electro-oxidation: Preparation, properties and characterisation, J. Power Sources 235 (2013) 111–116.
[26] S. Yao, G. Li, C. Liu, W. Xing, Enhanced catalytic performance of carbon supported palladium nanoparticles by in-situ synthesis for formic acid electrooxidation, J. Power Sources 284 (2015) 355–360.
[27] D. Bin, B. Yang, F. Ren, K. Zhang, P. Yang, Y. Du, Facile synthesis of PdNi nanowire networks supported on reduced graphene oxide with enhanced catalytic performance for formic acid oxidation, J. Mater. Chem. A 3 (26) (2015) 14001–14006.
[28] B.A. Al-Qodami, H.H. Alalawy, I.M. Al-Akraa, S.Y. Sayed, N. K. Allam, A.M. Mohammad, Surface engineering of nanotubular ferric oxyhydroxide "goethite" on platinum anodes for durable formic acid fuel cells, Int. J. Hydrog. Energy 47 (1) (2022) 264–275.
[29] Y. Sun, B. Huang, Y. Li, Y. Qin, Z. Fu, M. Sun, L. Wang, S. Guo, Segmented Au/PtCo heterojunction nanowires for efficient formic acid oxidation catalysis, Fundam. res. 1 (4) (2021) 453–460.
[30] S. Luo, W. Chen, Y. Cheng, X. Song, Q. Wu, L. Li, Trimetallic synergy in intermetallic PtSnBi nanoplates boosts formic acid oxidation, Adv. Mater. 31 (2019) 1903683.
[31] R. Zhang, M. Peng, L. Ling, B. Wang, PdIn intermetallic material with isolated single-atom Pd sites – A promising catalyst for direct formic acid fuel cell, Chem. Eng. Sci. 199 (2019) 64–78.
[32] I.M. Al-Akraa, A.M. Mohammad, A spin-coated TiOx/Pt nanolayered anodic catalyst for the direct formic acid fuel cells, Arab. J. Chem. 13 (3) (2020) 4703–4711.
[33] A.M. Mohammad, I.M. Al-Akraa, M.S. El-Deab, Superior electrocatalysis of formic acid electro-oxidation on a platinum, gold and manganese oxide nanoparticle-based ternary catalyst, Int. J. Hydrog. Energy 43 (1) (2018) 139–149.
[34] I.M. Al-Akraa, A.M. Mohammad, M.S. El-Deab, B.E. El-Anadouli, Electrooxidation of formic acid at platinum-gold nanoparticle-modified electrodes, Chem. Lett. 40 (12) (2011) 1374–1375.
[35] T. Zeng, X. Meng, H. Huang, L. Zheng, H. Chen, Y. Zhang, Controllable synthesis of web-footed PdCu nanosheets and their electrocatalytic applications, Small 18 (2022) 2107623.
[36] L.Y. Zhang, C.X. Guo, H. Cao, S. Wang, Y. Ouyang, B. Xu, Highly wrinkled palladium nanosheets as advanced electrocatalysts for the oxygen reduction reaction in acidic medium, Chem. Eng. J. 431 (2022) 133237.
[37] X. Zhang, J. Zhu, C.S. Tiwary, Z. Ma, H. Huang, J. Zhang, Z. Lu, W. Huang, Y. Wu, Palladium nanoparticles supported on nitrogen and sulfur dual-doped graphene as highly active electrocatalysts for formic acid and methanol oxidation, ACS Appl. Mater. Interfaces. 8 (17) (2016) 10858–10865.
[38] Y. Zhu, Y. Pan, Y. Zhu, H. Jiang, J. Shen, C. Li, Efficient electrocatalytic formic acid oxidation over PdAu-manganese oxide/carbon, J. Colloid Interface Sci. 593 (2021) 244–250.
[39] Z.-Y. Yu, R. Huang, J. Liu, C.-X. Luo, C.-Y. Wang, Q.-T. Song, PdPt concave nanocubes directly electrodeposited on carbon paper as high active and durable catalysts for formic acid and ethanol oxidation, Electrochim. Acta 354 (2020) 136654.
[40] C. Rettenmaier, R.M. Arán-Ais, J. Timoshenko, R. Rizo, H.S. Jeon, S. Kühl, S.W. Chee, A. Bergmann, B. Roldan Cuenya, Enhanced formic acid oxidation over SnO2-decorated Pd nanocubes, ACS Catal. 10 (24) (2020) 14540–14551.
[41] L.Y. Zhang, X. Meng, W. Zhang, T. Zeng, W. Yuan, Z. Zhao, Synthesis of palladium-tungsten metallene-constructed sandwich-like nanosheets as bifunctional catalysts for direct formic acid fuel cells, ACS Appl. Energy Mater. 4 (11) (2021) 12336–12344.
[42] X. Meng, T. Zeng, S. Ma, L. Zheng, H. Chen, W. Yuan, Surface nitridation of PdCu nanosheets to promote charge transfer and suppress CO poisoning toward ethanol electrooxidation, Adv. Mater. Interfaces 9 (2022) 2101849.

[43] I.M. Al-Akraa, Efficient electro-oxidation of formic acid at Pd-MnOx binary nanocatalyst: Optimization of deposition strategy, Int. J. Hydrog. Energy 42 (7) (2017) 4660–4666.
[44] S. Li, D. Cheng, X. Qiu, D. Cao, Synthesis of Cu@Pd core-shell nanowires with enhanced activity and stability for formic acid oxidation, Electrochim. Acta 143 (2014) 44–48.
[45] R. Ojani, Z. Abkar, E. Hasheminejad, J.-B. Raoof, Rapid fabrication of Cu/Pd nano/micro-particles porous-structured catalyst using hydrogen bubbles dynamic template and their enhanced catalytic performance for formic acid electrooxidation, Int. J. Hydrog. Energy 39 (15) (2014) 7788–7797.
[46] Y. Suo, I.-M. Hsing, Synthesis of bimetallic PdAu nanoparticles for formic acid oxidation, Electrochim. Acta 56 (5) (2011) 2174–2183.
[47] H. Wang, Y. Li, C. Li, Z. Wang, Y. Xu, X. Li, Hyperbranched PdRu nanospine assemblies: an efficient electrocatalyst for formic acid oxidation, J. Mater. Chem. A 6 (2018) 17514–17518.
[48] S. Yang, Y. Chung, K.-S. Lee, Y. Kwon, Enhancements in catalytic activity and duration of PdFe bimetallic catalysts and their use in direct formic acid fuel cells, J. Ind. Eng. Chem. 90 (2020) 351–357.
[49] H. Hosseini, M. Mahyari, A. Bagheri, A. Shaabani, Pd and PdCo alloy nanoparticles supported on polypropylenimine dendrimer-grafted graphene: A highly efficient anodic catalyst for direct formic acid fuel cells, J. Power Sources 247 (2014) 70–77.
[50] Y. Bao, M. Zha, P. Sun, G. Hu, L. Feng, PdNi/N-doped graphene aerogel with over wide potential activity for formic acid electrooxidation, J. Energy Chem. 59 (2021) 748–754.
[51] M.A. Matin, J.-H. Jang, Y.-U. Kwon, PdM nanoparticles (M = Ni Co, Fe, Mn) with high activity and stability in formic acid oxidation synthesized by sonochemical reactions, J. Power Sources 262 (2014) 356–363.
[52] Z. Chen, J. Zhang, Y. Zhang, Y. Liu, X. Han, C. Zhong, W. Hu, Y. Deng, NiO-induced synthesis of PdNi bimetallic hollow nanocrystals with enhanced electrocatalytic activities toward ethanol and formic acid oxidation, Nano Energy 42 (2017) 353–362.
[53] Y.-L. Fang, K.N. Heck, Z. Zhao, L.A. Pretzer, N. Guo, T. Wu, J.T. Miller, M.S. Wong, Gold-doping of carbon-supported palladium improves reduction catalysis, Chinese J. Catal. 37 (10) (2016) 1776–1786.
[54] Y.M. Asal, I.M. Al-Akraa, A.M. Mohammad, M.S. El-Deab, Design of efficient bimetallic Pt–Au nanoparticle-based anodes for direct formic acid fuel cells, Int. J. Hydrog. Energy 44 (7) (2019) 3615–3624.
[55] I.M. Al-Akraa, A.M. Mohammad, M.S. El-Deab, B.E. El-Anadouli, Electrocatalysis by nanoparticle: enhanced electro-oxidation of formic acid at NiOx–Pd binary nanocatalysts, J. Electrochem. Soc. 162 (2015) F1114-F1118.
[56] Y.M. Asal, A.M. Mohammad, S.S. Abd El Rehim, I.M. Al-Akraa, Preparation of Co-electrodeposited Pd-Au nanocatalyst for methanol electro-oxidation, Int. J. Electrochem. Sci. 16 (2021) Article Number: 211133.
[57] Y.M. Asal, A.M. Mohammad, S.S. Abd El Rehim, I.M. Al-Akraa, Synergistic enhancement of formic acid electro-oxidation on PtxCuy co-electrodeposited binary catalysts, J. Saudi Chem. Soc. 26 (2022) 101437.
[58] I.M. Al-Akraa, M.M. Mamdouh, Y.M. Asal, A.M. Mohammad, S.L. Rokhum, A competent MWCNT-grafted MnOx/Pt nanoanode for the direct formic acid fuel cells, J. Chem. 2022 (2022) 1–11.
[59] I.M. Al-Akraa, A.M. Mohammad, M.S. El-Deab, B.E. El-Anadouli, Electrocatalysis by design: Synergistic catalytic enhancement of formic acid electro-oxidation at core–shell Pd/Pt nanocatalysts, Int. J. Hydrog. Energy 40 (2015) 1789–1794.
[60] I.M. Al-Akraa, A.M. Mohammad, M.S. El-Deab, B.E. El-Anadouli, Fabrication of CuO x-Pd nanocatalyst supported on a glassy carbon electrode for enhanced formic acid electro-oxidation, J. Nanotechnol. 2018 (2018) 1–9.
[61] I.M. Al-Akraa, A.M. Mohammad, M.S. El-Deab, B.E. El-Anadouli, Advances in direct formic acid fuel cells: fabrication of efficient Ir/Pd nanocatalysts for formic acid electro-oxidation, Int J Electrochem Sci. 10 (2015) 3282–3290.
[62] Y. Wang, Z. Xiong, Y. Xia, Branched PdAu nanowires with superior electrocatalytic formic acid oxidation activities, RSC Adv. 7 (64) (2017) 40462–40469.
[63] K. Jurkiewicz, M. Pawlyta, A. Burian, Structure of carbon materials explored by local transmission electron microscopy and global powder diffraction probes, Carbon 4 (2018) 68.
[64] B. Zhang, D. Ye, J. Li, X. Zhu, Q. Liao, Electrodeposition of Pd catalyst layer on graphite rod electrodes for direct formic acid oxidation, J. Power Sources 214 (2012) 277–284.
[65] S.M. Baik, J. Han, J. Kim, Y. Kwon, Effect of deactivation and reactivation of palladium anode catalyst on performance of direct formic acid fuel cell (DFAFC), Int. J. Hydrog. Energy 36 (22) (2011) 14719–14724.
[66] A. Gharib, A. Arab, Electrodeposited Pd, PdCd, and PdBi nanostructures: Preparation, characterization, corrosion behavior, and their electrocatalytic activities for formic acid oxidation, J. Electroanal. Chem. 866 (2020) 114166.
[67] G.A. El-Nagar, A.M. Mohammad, M.S. El-Deab, B.E. El-Anadouli, Novel fuel blends facilitating the electro-oxidation of formic acid at a nano-Pt/GC electrode, RSC Adv. 6 (35) (2016) 29099–29105.
[68] G.H. El-Nowihy, M.S. El-Deab, Smart selection of fuel blends: Robust oxidation of formic acid in its blend with urea at NiOx/Pd nanoparticles-based binary anodes, Renew. Energy. 167 (2021) 830–840.
[69] R. Kottayintavida, N.K. Gopalan, PdAu alloy nano wires for the elevated alcohol electro-oxidation reaction, Electrochim. Acta 384 (2021) 138405.
[70] P. Hong, F. Luo, S. Liao, J. Zeng, Effects of Pt/C, Pd/C and PdPt/C anode catalysts on the performance and stability of air breathing direct formic acid fuel cells, Int. J. Hydrog. Energy 36 (14) (2011) 8518–8524.
[71] W.S. Jung, J. Han, Enhanced stability of PdPtAu alloy catalyst for formic acid oxidation, Korean J. Chem. Eng. 38 (11) (2021) 2229–2234.
[72] Y. Tang, S. Zou, Formic acid oxidation on Pd thin film coated Au nanocrystals, Surfaces. 2 (2019) 372–386.
[73] Y. Wang, T.S. Nguyen, X. Liu, X. Wang, Novel palladium–lead (Pd–Pb/C) bimetallic catalysts for electrooxidation of ethanol in alkaline media, J. Power Sources 195 (9) (2010) 2619–2622.
[74] F. Gao, D.W. Goodman, Pd–Au bimetallic catalysts: understanding alloy effects from planar models and (supported) nanoparticles, Chem. Soc. Rev. 41 (2012) 8009–8020.
[75] D.V. Ribeiro, C.A.C. Souza, J.C.C. Abrantes, Use of Electrochemical Impedance Spectroscopy (EIS) to monitoring the corrosion of reinforced concrete concrete, Rev IBRACON Estrut Mater. 8 (4) (2015) 529–546.
[76] L.Y. Zhang, F. Wang, S. Wang, H. Huang, X. Meng, Y. Ouyang, Layered and heterostructured Pd/PdWCr sheet-assembled nanoflowers as highly active and stable electrocatalysts for formic acid oxidation, Adv. Funct. Mater. 30 (2020) 2003933.
[77] L.Y. Zhang, Z.L. Zhao, C.M. Li, Formic acid-reduced ultrasmall Pd nanocrystals on graphene to provide superior electocatalytic activity and stability toward formic acid oxidation, Nano Energy 11 (2015) 71–77.